Received: 6 July 2020 | Revised: 10 August 2020 | Accepted: 11 August 2020

DOI: 10.1111/jnc.15155

ORIGINAL ARTICLE

Journal of Neurochemistry JNC The Official Journal of the International Society for Neurochemistry WILEY

Central cholinergic function and metabolic changes in streptozotocin-induced rat brain injury

Tri Yuliani[1,2] | Sebastian Lobentanzer[1] | Jochen Klein[1]

[1]Institute of Pharmacology and Clinical Pharmacy, College of Pharmacy, Goethe University, Frankfurt am Main, Germany

[2]Research Center for Chemistry, Indonesian Institute of Sciences (LIPI), Tangerang Selatan, Banten, Indonesia

Correspondence
Jochen Klein, Institute of Pharmacology and Clinical Pharmacy, College of Pharmacy, Biocenter N260, Max-von-Laue Str. 9, Goethe University Frankfurt, 60438 Frankfurt am Main, Germany.
Email: klein@em.uni-frankfurt.de

This article is part of the Special Issue "Cholinergic Mechanisms".

Abstract

As glucose hypometabolism in the brain is an early sign of Alzheimer´s dementia (AD), the diabetogenic drug streptozotocin (STZ) has been used to induce Alzheimer-like pathology in rat brain by intracereboventricular injection (icv-STZ). However, many details of the pathological mechanism of STZ in this AD model remain unclear. Here, we report metabolic and cholinergic effects of icv-STZ using microdialysis in freely moving animals. We found that icv-STZ at a dose of 3 mg/kg (2 × 1.5 mg/kg) causes overt toxicity reflected in body weight loss. Three weeks after STZ administration, histological examination revealed a high number of glial fibrillary acidic protein reactive cells in the hippocampus, accompanied by Fluoro-Jade C-positive cells in the CA1 region. Glucose and lactate levels in microdialysates were unchanged, but mitochondrial respiration measured ex vivo was reduced by 9%–15%. High-affinity choline uptake, choline acetyltransferase, and acetylcholine esterase (AChE) activities in the hippocampus were reduced by 16%, 28%, and 30%, respectively. Importantly, extracellular acetylcholine (ACh) levels in the hippocampus were unchanged and responded to behavioral and pharmacological challenges. In comparison, extracellular ACh levels and cholinergic parameters in the striatum were unchanged or slightly increased. We conclude that the icv-STZ model poorly reflects central cholinergic dysfunction, an important characteristic of dementia. The icv-STZ model may be more aptly described as an animal model of hippocampal gliosis.

KEYWORDS

acetylcholine, Alzheimer's disease, astrogliosis, complex IV, glucose, hippocampus, lactate, microdialysis, mitochondrial respiration, streptozotocin

Abbreviations: ACh, acetylcholine; AChE, acetylcholine esterase; aCSF, artificial cerebrospinal fluid; AD, Alzheimer's disease; BSA, bovine serum albumine; ChAT, choline acetyltransferase; CHT-1, high-affinity choline transporter 1; CS, citrate synthase; ETC, electron transport chain; FJ, Fluoro-Jade C; GFAP, glial fibrillary acidic protein; HACU, high-affinity choline reuptake; HPC, hippocampus; HPLC, high-performance liquid chromatography; icv, intracerebroventricular; PBS, phosphate-buffered saline; PFA, paraformaldehyde; RRID, Research Resource Identifier (see scicrunch.org); STR, striatum; STZ, Streptozotocin.

1 | INTRODUCTION

Animal models are of great importance to understand Alzheimer's disease (AD) pathology and to evaluate potential therapies, but can also be misleading if they do not adequately reflect human disease (Drummond & Wisniewski, 2017). While transgenic approaches imitate early-onset AD only, toxic models may more closely mimic the typical, late-onset dementia in humans (Cavanaugh, Pippin, & Barnard, 2014). One such model in which brain injury is induced by intracerebroventricular injection of streptozotocin in rats (icv-STZ), was developed based on the idea that AD resembles "diabetes of the brain", and is caused by an insulin-resistant brain state (Hoyer, 1998; de la Monte & Tong, 2014). Insulin can cross the blood–brain barrier (Banks, Owen, & Erickson, 2014) and insulin receptors are widely expressed in the brain, e.g., occurring in hippocampus and striatum (Arnold et al., 2018). Recent studies indicate that insulin contributes to cognition in animals and is being tested as a possible therapeutic option in AD (Clarke, Ribeiro, Frozza, De Felice, & Lourenco, 2018; Grillo et al., 2015). The icv-STZ model induces AD-like symptoms such as memory impairment, glucose hypometabolism, mitochondrial dysfunction, increased oxidative stress, neuroinflammation, and neurodegeneration (Knezovic et al., 2015; Salkovic-Petrisic & Hoyer, 2007). More than 50 studies have used this model to investigate potential therapeutic effects of a variety of drugs, including lithium, NMDA receptor antagonists, antioxidants, pioglitazone, and many more (reviewed by Salkovic-Petrisic, Knezovic, Hoyer, & Riederer, 2013).

Two aspects of this model, however, have not been thoroughly investigated. First, the mechanism of STZ action in the brain remains unknown. In the periphery, STZ is taken up into cells (e.g., pancreatic ß-cells) preferentially via the GLUT2 glucose transporter receptor (SLC2A2) which is poorly expressed in the brain. The effects of insulin on blood glucose are mediated by the GLUT4 glucose transporter (SLC2A4). In the brain, however, the insulin-insensitive glucose transporters GLUT1 and 3 are predominant, with GLUT1 preferentially expressed in endothelia and glial cells and GLUT3 in neurons. Second, in humans, central cholinergic dysfunction is closely associated with cognitive function (Ballinger, Ananth, Talmage, & Role, 2016), and current drug treatment of AD is largely dependent on acetylcholinesterase (AChE) inhibitors which increase acetylcholine (ACh) levels in the brain. However, the effects of icv-STZ administration on central cholinergic systems have not been investigated in depth. Some studies determined activities of choline acetyltransferase (ChAT) or acetylcholinesterase (AChE), but these enzymatic activities do not correlate with ACh release. After icv-STZ administration, ChAT activity was reduced in the hippocampus to varying degrees, but was unchanged in the septum (Hellweg, Nitsch, Hock, Jaksch, & Hoyer, 1992; Terwel, Prickaerts, Meng, & Jolles, 1995). ChAT-positive cells were reduced in one study in the basal forebrain (Majkutewicz et al., 2016). AChE activity was found to be increased, and total ACh levels decreased, in some studies (Costa et al., 2016; Sorial & El-Sayed, 2017), but both measurements were done in brain homogenates and, therefore, poorly reflect local cholinergic activity. Another study reported an unchanged number of basal forebrain cholinergic neurons (based on ChAT immunoreactivity) or hippocampal cholinergic terminals (based on vesicular acetylcholine transporter (VAChT) staining) (Shoham, Bejar, Kovalev, Schorer-Apelbaum, & Weinstock, 2007). As cholinergic dysfunction is an important characteristic of AD, a more detailed investigation into cholinergic activity seemed warranted. We here report microdialysis findings of cholinergic activity in icv-STZ-treated rats, and we compare our findings with metabolite and mitochondrial data to monitor changes in energy metabolism.

2 | MATERIALS AND METHODS

2.1 | Animals and treatments

Icv-STZ-induced brain injury was induced in male Wistar rats (RRID:RGD_13508588) of 150–250 g body weight (5 weeks of age; Janvier Labs, Le Geneste St. Isle, France). A total of 103 rats were housed in a controlled room (22°C, 50%–65% humidity; day/night cycle of 12/12 hr) with free access to water and standard laboratory diet (Altromin; 1324, 2018) and were numbered Rat 1 to Rat 103. After 7 days of acclimatization, they were divided into 2 or 3 groups per cage and block randomization according to 3 or 4 rats per cage was used. Rats were divided to receive different treatment in the following order. For two groups per cage: AACC, ACCA, ACAC, CAAC, CACA, and CCAA. For three groups per cage: ABC, ACB, BAC, BCA, CAB, and CBA (Table S1).

For treatments, the high-dose group (group C) received icv-STZ twice at a dose of 1.5 mg/kg (Sigma-Aldrich S0130, 2018) dissolved in water (Fresenius Kabi, 406760000, 2018) on day 0 and day 3. The low-dose group (group B) received icv-STZ once at a dose of 0.6 mg/kg in saline. The control group (group A) received saline twice on days 0 and 3 (B. Braun, 2350720, 2018). Freshly prepared streptozotocin maintains its effects at neutral pH as reviewed by Deeds et al. (2011). During the experiments, the experimenter was unaware of the animal's group during raw data calculation and data analysis because during those times, the rats were labeled as number 1–103 by another researcher, and de-blinding occurred after data analysis.

Icv infusions (5 µl) were performed for 5 min into brain lateral ventricles in fully anaesthetized rats using isoflurane (Iso-vet, 3949, 2018; induction dose 5%, maintenance dose 1.5%–2% v/v) in synthetic air (Air Liquide, 6716684, 2018, Düsseldorf, Germany). Isofluran was used because of rapid recovery, lower incidence of death, and rapid elimination. The coordinates used in the stereotaxic instrument (Stoelting, Chicago, IL, USA) were as follows: AP: −0.8 mm; L: ±1.5 mm; and DV: −3.6 mm (Paxinos & Watson, 1998). Bupivacain (Jenapharm, 30004090000, 2018) was applied for long-lasting local anesthesia. The diffusion of drugs was confirmed by an infusion of fast green dye (Sigma-Aldrich F7258, 2018). Health status was monitored daily and body weights were checked twice a week for 21 days before experiments. The distribution of the 103 rats into experimental groups is illustrated in Table S1. As described

above, the rats received saline or STZ (1.5 mg/kg) by i.c.v. injection on days 0 and 3. In the case of the low-dose STZ group, 0.6 mg/kg was administered once by i.c.v. infusion on day 0. This low dose of icv-STZ was only used for microdialysis studies. On day 20 after the initial injection, microdialysis probes were inserted under isoflurane anesthesia as described below. On days 21 and 22, microdialysis experiments were performed (day 21: open field; day 22: scopolamine). A total of 45 rats were used for this part of the study, but because of blocked probes, 3 rats had to be excluded from analysis so that 42 rats were entered into data analysis. For the other experimental procedures, only two groups of rats were used, saline-treated rats and rats that received high-dose STZ. We used two groups of 9 rats each for histology, two groups of 8 rats each for the measurement of cholinergic parameters, and two groups of 12 rats each for measurement of mitochondrial activities. The flow diagram of the experiments is illustrated in Figure 1.

Both animal treatments and experiments were done in mixed order (saline, STZ; STZ, saline). Experiments were carried out according to the German Law for Animal Protection and were registered with Regierungspräsidium Darmstadt (FR/1005). The experimenter was unaware of the animal's group during raw data calculation and data analysis. The study was not pre-registered and exploratory.

2.2 | Histology and immunohistochemistry

Nine rats of the saline group and 9 rats of the high-dose STZ group were killed by intraperitoneal injection of ketamine (2 × 80 mg/kg; Inresa, 07714091, 2018) and xylazine (2 × 10 mg/kg; Bayer, 770–081, 2018) and transcardially perfused with 500 ml 4°C saline (Braun, 8779253, 2018) and 400 ml 4% paraformaldehyde (Merck 104005, 2018) in phosphate-buffered saline (PBS) (Gerfen, 2003). A combination of ketamine and xylazine was used because of its beneficial cardiovascular effects. The brain was collected and 3 mm coronal sections were made followed by post-fixation in 4% paraformaldehyde in PBS for 4 hr. Sections were transferred to 20% sucrose (Sigma-Aldrich, S0389, 2018) in PBS at 4°C. The sections were then frozen in Tissue-Tek® O.C.T mounting medium (Sakura, 4583, 2018) and 14 µm coronal sections were cut and spread on microscope slides and allowed to air-dry. GFAP staining was performed according to Kallenborn-Gerhardt et al. (2014). Air-dried sections were washed in PBS for 3 × 10 min, permeabilized in PBS containing 0.1% Triton X-100 (Sigma-Aldrich, T8787, 2018) for 5 min, and blocked in PBS containing 10% normal goat serum (Sigma-Aldrich, G9023, 2018) and 3% bovine serum albumine (Carl Roth, 3737.1, 2018) for 60 min. Next, sections were incubated with primary antibody overnight at 4°C (rabbit anti-GFAP, 1:1,000, Agilent Cat# Z0334, RRID:AB_10013382). After three washes in PBS, the sections were incubated in secondary antibody for 2 hr in the dark (goat anti-rabbit IgG AF555, 1:500, Molecular Probes Cat# A-21429, RRID:AB_141761) followed by three washes. Next, quenching was done using 0.06% Sudan black B (Sigma-Aldrich, 199664, 2018) in 70% ethanol (Fisher Chemical, E/0665DF/15, 2018) for 5 min followed by three washes. Coverslips were mounted using Fluoromount G (Invitrogen, 00-4958-02, 2018).

Fluoro-Jade C staining (Merck, AG 325, 2018) was performed based on Schmued, Stowers, Scallet, and Xu (2005). Air-dried sections were soaked in 70% ethanol for 3 min followed by three washes in milli-Q water. Next, sections were soaked in 0.06% $KMnO_4$ (Sigma-Aldrich, 223468, 2018) for 15 min followed by three washes. Sections were then stained using 0.0001% Fluoro-Jade C in 0.1% acetic acid (Sigma-Aldrich, 1000631011, 2018) for 15 min followed by three washes and air-drying over night at 20°C. Air-dried sections were cleared in xylene and coverslips were mounted using DPX (Sigma-Aldrich, 06522, 2018).

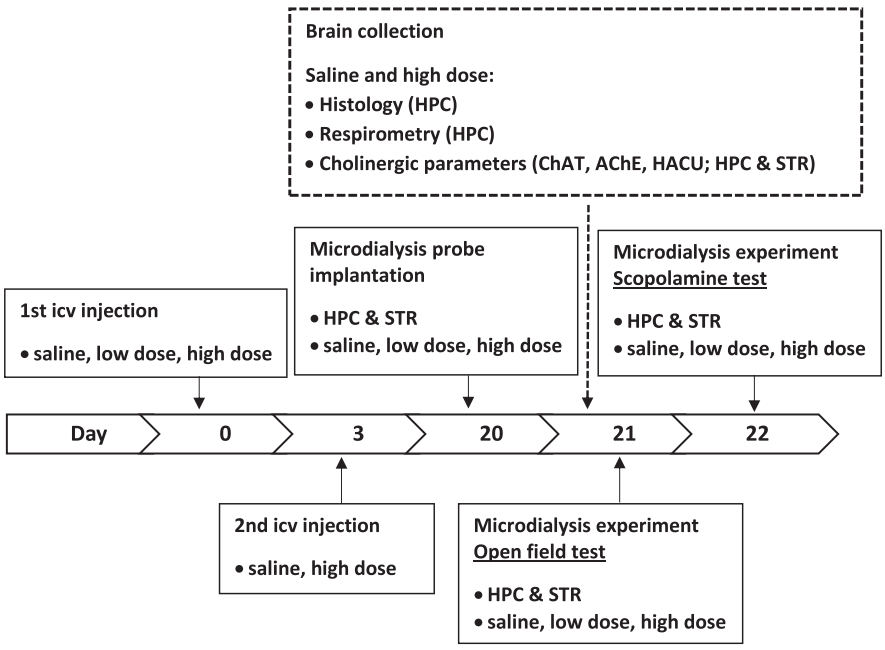

FIGURE 1 Flow diagram of the experiments. HPC = hippocampus; STR = striatum. For microdialysis experiments, different brain regions (HPC or STR) used different rats. Experiments in the dashed box used different rats for each experiment except cholinergic parameter experiments in which the hippocampus and striatum samples were obtained from the same rats

The fluorescence signal was detected using a FITC (Fluorescein isothiocyanate) filter (Semrock) for Fluoro-Jade C and TRITC (Tetramethylrhodamine) filter (Semrock) for GFAP. Pictures were processed by Nikon software NIS-Elements and combined by Adobe Photoshop CS. Fluorescence intensity was quantified by ImageJ software.

2.3 | Mitochondrial oxygen consumption

Twenty-one days after the first icv-STZ injection, hippocampi of 24 rats (12 rats of the saline group and 12 rats of the high-dose STZ group) were collected quickly after decapitation and mitochondria were isolated according to Hagl et al. (2013). Mitochondrial oxygen consumption was measured using Oroboros Oxygraph-2K (O2K) (Gnaiger, 2014). Briefly, the O2K chambers were filled with 2 ml of MiR05 medium (110 mM sucrose, 60 mM K lactobionate, 0.5 mM EGTA, 3 mM $MgCl_2$, 20 mM taurine, 10 mM KH_2PO_4, 20 mM HEPES, and 1 g/L bovine serum albumine essentially fatty acid-free) and 80 µl of isolated mitochondria. Activities of electron transport chain complexes were determined using an established substrate/uncoupler/inhibitor titration (SUIT) protocol. Complex I activity was measured after the addition of pyruvate (5 mM; Sigma-Aldrich, P2256, 2018), malate (2 mM; Sigma-Aldrich, M1000, 2018), and ADP (2 mM; Sigma-Aldrich, A5285, 2018). Then, complex V activity was inhibited by the addition of oligomycin (2 µg/ml; Sigma-Aldrich, O4876, 2018). Maximum electron transfer (complex III) was measured after the addition of FCCP (protonophore; Sigma-Aldrich, C2920, 2018). Complex II activity was measured after inhibition of Complex I by the addition of rotenone (0.5 µM; Sigma-Aldrich, R8875, 2018). Then, mitochondrial respiration was blocked by the addition of antimycin-A (Sigma-Aldrich, A8674, 2018) which inhibits complex III. Maximum complex IV activity was measured after the addition of tetramethyl-phenylenediamine (TMPD; 0.5 mM; Sigma-Aldrich, A7631, 2018) as electron donor and 2 mM ascorbate (Sigma-Aldrich, A7631, 2018) to maintain the reduced state of TMPD. Finally, citrate synthase (CS) activity was measured by a colorimetric assay as described by Hagl et al. (2013) and complex activities were expressed relative to CS activities.

2.4 | Microdialysis of metabolites and acetylcholine

Y-shaped, concentric microdialysis probes (Polysulfone membrane FX CorDiax 600, Fresenius Medical Care, 0123, 2017) with a molecular weight cutoff of 30 kDa and an exchange area of 3 mm were manufactured as described previously (Lietsche, Gorka, Hardt, Karas, & Klein, 2014; RRID: SCR_018571) and implanted in the hippocampus or striatum of fully anaesthetized rats (for pain relief, bupivacaine and isoflurane were used as described above). The following coordinates from bregma were used (hippocampus AP: −5.2 mm; L: −4.8 mm; DV: −7.0 mm; STR AP: +0.2 mm; L: −2.8 mm; DV: −7.5 mm) (Paxinos & Watson, 1998). A total of 45 rats from three groups (saline, low-dose STZ, and high-dose STZ of 15 rats each) were used in this study. The rats were divided into hippocampus experiment (21 rats; 7 rats each group) and striatum experiments (24 rats; 8 rats each group).

Rats were allowed to recover over night and microdialysis experiments were conducted for 2 days after probe implantation between 09:00 and 17:00 hr. The probes were perfused with artificial cerebrospinal fluid (147 mM NaCl, 4 mM KCl, 1.2 mM $CaCl_2$, and 1.2 mM $MgCl_2$) at a rate of 2 µl/min. After 30 min of equilibrium between perfusion liquid and tissue, dialysates of 15 min intervals were collected for 90 min (6 × 30 µL) and used for analysis. For extracellular acetylcholine level measurement, the artificial cerebrospinal fluid was supplemented with 0.1 µM neostigmine (Sigma-Aldrich, N2001, 2015) to stabilize extracellular levels of ACh. After collection of the first 90 min dialysates (basal data), rats were moved to an open field box (35 × 32 × 20 cm) as exploration and increased locomotor activity are known to physiologically stimulate hippocampal ACh release (König, Berlin, et al., 2018). After collection of the second 90 min dialysates, the rats were transferred back to the microdialysis cage and dialysates were collected for another 90 min.

On day 2, after collection of dialysates under basal conditions, 1 µM scopolamine (Sigma-Aldrich, S0929, 2015) was added to the perfusion solution to pharmacologically stimulate ACh release, and dialysates were collected for 90 min followed by another 90 min of dialysis without scopolamine. Afterwards, rats were killed in isoflurane anesthesia and the brains were removed for further analysis and probe location confirmation.

2.5 | Determination of metabolites

Glucose, lactate, pyruvate, and glycerol levels in dialysates were measured by enzymatic reaction and colorimetric method using CMA 600 and an Iscus® microdialysate analyzers. ß-Hydroxybutyrate was determined by GC-MS and isoprostane levels by ELISA (8-isoprostane express EIA kit®, Cayman Chemicals, 516360, 2019), as previously described (Imran, Hillert, & Klein, 2015; Koch et al., 2017).

2.6 | Determination of acetylcholine and choline

ACh and choline levels were determined by directly injecting 10 µl dialysate into a high-performance liquid chromatograph coupled with an electrochemical detector system (HPLC-ECD). The system consisted of an autosampler, a pump with degasser, a pre-column, a separation column, an enzyme reactor (AChE and choline oxidase), and an electrochemical detector (a platinum electrode working at + 500 mV by Eicom, Kyoto, Japan). The mobile phase consisted of $KHCO_3$ 50 mM, EDTA-Na_2 134.3 mM, and sodium

decane-1-sulfonate 1.64 mM in RotisolV® HPLC gradient grade water with a pH of 8.4 and flow rate at 150 µl/min.

2.7 | Cholinergic parameters (HACU, ChAT, AChE)

A total of 16 rats from the saline group and high-dose STZ group (8 rats each) were used for the study of cholinergic parameters. The hippocampus and striatum were collected from each rat and homogenates of each brain region were made. Each homogenate was divided into three subsamples for HACU, ChAT, and AChE studies.

High-affinity choline uptake (HACU) mediated by the choline transporter-1 (CHT-1) was determined based on König, Berlin, et al. (2018). Briefly, hippocampal homogenate in HEPES/sucrose buffer was centrifuged at 17,000 *g* for 10 min at 4°C to collect the P2 fraction containing synaptosomes. It was then incubated with or without 1 µM hemicholinium-3 (HC-3; Sigma-Aldrich, H108, 2018) in Krebs-Henseleit buffer (KHB; containing NaCl 115 mM, KCl 7.1 mM, $CaCl_2$ 1.2 mM, $MgSO_4$ 1.2 mM, $NaHCO_3$ 25 mM, Na_2HPO_4 1.5 mM, glucose 12.8 mM, and saturated with carbogen to pH 7.2–7.4) containing 5 µCi ^{3}H-choline 50 nM (American Radiolabeled Chemicals, 0197, 2018). Choline uptake was stopped by the addition of 1 ml of ice-cold KHB followed by centrifugation. After washing with KHB, the pellet was resuspended in methanol to disintegrate the membranes. The released ^{3}H-choline was then measured using a scintillation counter (Wallac system 1409, Perkin Elmer). The HC-3-sensitive high-affinity choline uptake was calculated based on the difference in uptake with or without HC-3 and expressed as dpm/µg protein. Protein content was determined by the Bradford method (Bradford, 1976).

Choline acetyltransferase (ChAT) activity was measured using ^{3}H-acetyl-CoA (American Radiolabeled Chemicals, 0204, 2018) and choline (Sigma-Aldrich, C7017, 2018) as the substrate (Fonnum, 1969). Briefly, hippocampal homogenates containing 0.25 µg/µL protein were added to a reaction mix (0.5% Triton X-100, 0.3 M NaCl, 0.02 M EDTA, 0.05 M Na_3PO_4 pH 7.4, 2 mM choline chloride, 1 mM neostigmine bromide, and 0.5 mCi ^{3}H-acetyl coenzyme A). After incubation at 37°C for 15 min, the reaction was stopped by ice-cold PBS (1 mM, pH 7.4). ^{3}H-ACh was extracted using 0.5% sodium tetraphenylborate in 85:15 toluene:acetonitrile. After centrifugation, the supernatant was collected for measurement of radioactivity.

Acetylcholinesterase (AChE) activity was measured based on Ellman, Courtney, Andres, and Featherstone (1961). Briefly, hippocampal homogenate in HEPES/sucrose buffer was permeabilized with 0.5% Triton-X. After centrifugation, the supernatant was mixed with Ellman buffer (0.1 M NaH_2PO_4, 0.1 M Na_2HPO_4, pH 8) and iso-OMPA (final concentration 100 µM) to block butyryl-cholinesterase. After addition of acetylthiocholine and dithionitrobenzoic acid (1 mM and 500 µM final concentrations, respectively), the absorbance was measured at 405 nm using a Victor multi-label plate reader (Perkin Elmer, Bedford, USA). Enzyme activity was calculated using a standard curve and normalized with protein level (mU/µg protein) which was determined by the Bradford method (Bradford, 1976).

2.8 | Single-cell sequencing analyses

Raw single-cell expression data of the adult mouse nervous system (Zeisel et al., 2018) were downloaded from http://mousebrain.org/downloads.html in two resolution levels: at the single-cell level and at cell-type level. Data were imported into the R environment using R/loomR (https://github.com/mojaveazure/loomR) and R/LoomExperiment (Morgan & Van Twisk, 2019) and analyzed regarding cholinergic transcripts and glucose transporters. Results were visualized using R/ggplot2 (Wickham, 2016).

Correlation of expression of the selected genes was determined via Pearson's product–moment correlation coefficient (PPMCC, using the *cor()* function of R/stats). P-values for each PPMCC were calculated for the entire gene-sample matrix using the *cor_pmat()* function, and plotted using the *ggcorrplot()* function of R/ggcorrplot (https://github.com/kassambara/ ggcorrplot). Correlation was assumed significant at $p < .05$. All analyses were performed using R software version 3.5.1 ("Feather Spray").

2.9 | Statistical analysis

If not indicated otherwise, data are presented as means ± *SEM* of N animals. All data were tested for normal distribution by the Kolmogorov–Smirnov test (GraphPad Prism 5.03). Potential outliers (>2 *SD*) were identified by the Grubbs test (https://www.graphpad.com/quickcalcs/grubbs). Sample size was calculated using $N = 2\ SD^2 \times$ power index/ delta^2. From many years of experience with microdialysis, we expected an *SD* of 20% and a treatment effect of 25%. The value for the power index ($\alpha = 0.05$, two-sided; ß = 0.2; 80%) was taken from the book "Intuitive Statistics" by Harvey Motulsky (Oxford University Press, 1995). Time courses of body weight (Figure 2) and acetylcholine levels (Figure 5 and Figure 6) were compared using two-way analysis of variance for repeated measurements (ANOVA; GraphPad Prism 5.03; GraphPad Software, La Jolla, CA, USA) with Bonferroni's post-test for multiple pair-wise comparisons. One-way ANOVA followed by Tukey's multiple comparison test was used to compare means between three groups on basal values of metabolites (Table 1) and on metabolites (glucose, lactate; Figure S2). Means between two groups were compared by Student's *t*-test for mitochondrial respiration (Figure 4), cholinergic parameters (Tables 2 and 3), and quantification of fluorescence intensity (Figure S1). *p*-values <.05 were considered to be statistically significant. All data in Figures 2, 4-6, Tables 1–3, and Figure S1 and S2 were normally distributed, and no outliers were detected.

2.10 | Exclusion criteria

Table S1 shows the number of excluded animals as a result of failure in dialysates collection because of damaged probe during implantation or incorrect dialysates volume.

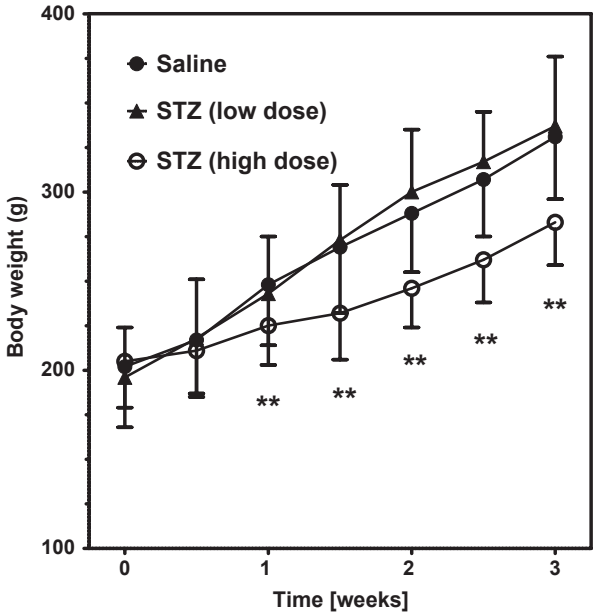

FIGURE 2 Body weight of rats after treatment with saline (twice) or streptozotocin (STZ) at low (once 0.6 mg/kg) or high (twice 1.5 mg/kg) doses. Data are means ± *SD* of *N* = 17–20 animals. Statistics: two-way ANOVA with Bonferroni post-test: $^{**}p < .01$ versus saline. Two-way ANOVA, saline versus. STZ (low dose): $F_{1,35} = 1.97$, $p = .17$; saline versus STZ (high dose): $F_{1,38} = 17.76$, $^{**}p < .01$

3 | RESULTS

3.1 | Icv-STZ induces toxicity, gliosis, and neurodegeneration in hippocampus

Icv-STZ was clearly toxic to the animals as seen in the development of body weight (Figure 2). While the rats developed normally after administration of the low dose (0.6 mg/kg STZ), there was initially no increase in body weight after administration of the high dose of icv-STZ, followed by a period of weight gain. At the end of the experiment (on day 21), high-dose STZ-treated rats had 15% less body weight compared to controls (saline 331 ± 35 g versus high dose 283 ± 24 g, *N* = 15; $p < .01$).

On day 21, rats were killed and histology was performed to monitor cellular toxicity. The immunohistochemical study with the GFAP primary antibody revealed glial activation after high-dose icv-STZ that was visible in both dorsal and ventral hippocampus, and especially at the CA1 region (Figure 3a and b). The quantification of GFAP staining showed a reproducible and highly significant increase in GFAP expression (Figure S1a). Fluoro-Jade C staining which indicates apoptosis was also positive in the hippocampal CA1 region, however, only 3 of 9 rats showed a strong response (Figure 3c and Figure S1b).

3.2 | Metabolic screening after icv-STZ

We used microdialysis to monitor various indicators of energy metabolism and cellular toxicity. We found that icv-STZ did not affect extracellular glucose levels in the brain (Figure S2a). There was also no significant change in glucose levels during behavioral or pharmacological stimulation (Figure S2a). Lactate levels in brain microdialysates were reduced by 24% after both low- as well as high-dose STZ (Figure S2b) while pyruvate levels were increased (Table 1), however, the changes were not statistically significant (Table 1). The extracellular concentration of ß-hydroxybutyrate (a ketone body) was unchanged (Table 1). Interestingly, glycerol and especially choline, both breakdown products of membrane phospholipids, were increased by STZ (Table 1; $p < .05$ for choline). The concentration of isoprostanes, which indicate lipid peroxidation and oxidative stress, was unchanged following STZ (Table 1).

In addition, we measured mitochondrial oxygen respiration in mitochondria that was isolated from rat hippocampi 21 days after high-dose icv-STZ. After normalization of the data for citrate synthase activity, all complexes showed a reduction in oxygen consumption by 9%–15% that was statistically significant for

TABLE 1 Extracellular concentrations of metabolites as determined by microdialysis under basal conditions (not corrected for recovery)

Metabolite	Saline	Low-dose STZ	High-dose STZ	*t*	*p*
Acetylcholine [nM]	8.71 ± 1.33	7.29 ± 0.84	7.48 ± 1.58	0.34	.72
Choline [μM]	0.69 ± 0.06	0.82 ± 0.07	0.94 ± 0.06 *	5.34	.02
Glucose [μM]	204 ± 29	202 ± 13	233 ± 25	0.57	.58
Lactate [μM]	192 ± 34	135 ± 20	150 ± 9	1.63	.22
Pyruvate [μM]	6.8 ± 0.9	11.6 ± 1.5	13.5 ± 2.5	3.80	.06
Glycerol [μM]	2.69 ± 0.38	3.77 ± 0.64	4.76 ± 1.07	1.60	.23
ß-Hydroxybutyrate [μM]	6.12 ± 1.23	6.85 ± 0.90	7.08 ± 0.84	0.26	.77
Isoprostanes [pg/ml]	26.4 ± 1.54	23.2 ± 2.2	31.4 ± 2.9	3.28	.06

Note: Data are means ± *SEM* (*N* = 6 animals) and were analyzed by one-way ANOVA followed by Tukey's multiple comparison test. $^{*}p < .05$ versus saline.

TABLE 2 Cholinergic parameters as determined in rat hippocampus 3 weeks after icv-STZ administration

Activity	Saline	High-dose STZ	*t*	*p*
Choline acetyltransferase (ChAT) (ACh nmol/h/mg protein)	39.67 ± 1.71	29.22 ± 2.49**	3.46	<.01
Acetylcholinesterase (AChE) (AChE mU/mg Protein)	111.2 ± 3.67	76.92 ± 8.02**	3.89	<.01
High-affinity choline uptake (HACU) (DPM/μg Protein)	358 ± 42	300 ± 30	1.08	.30
Low-affinity choline uptake (LACU) (DPM/μg Protein)	138 ± 8	139 ± 10	0.11	.92

**$p < .01$ versus saline. Data are means ± *SEM* ($N = 8$ animals) and were analyzed by unpaired *t*-test.

TABLE 3 Cholinergic parameters as determined in rat striatum 3 weeks after icv-STZ administration

Activity	Saline	High-dose STZ	*t*	*p*
Choline acetyltransferase (ChAT) (ACh nmol/h/mg protein)	97.83 ± 2.38	99.67 ± 3.24	0.46	.65
Acetylcholinesterase (AChE) (AChE mU/mg Protein)	411.1 ± 10.20	441.5 ± 10.35*	2.09	.05
High-affinity choline uptake (HACU) (DPM/μg Protein)	393 ± 13	514 ± 40*	2.73	.02
Low-affinity choline uptake (LACU) (DPM/μg Protein)	157 ± 7	153 ± 6	0.37	.72

*$p < .05$ versus saline. Data are means ± *SEM* ($N = 8$) animals and were analyzed by unpaired *t*-test.

complexes II (succinate dehydrogenase) and IV (cytochrome oxidase) (Figure 4).

3.3 | Central cholinergic activity after icv-STZ

To follow cholinergic activity in situ in real time, we used microdialysis and an HPLC-based, highly sensitive detection method for acetylcholine (ACh). The results of these studies are shown in Figure 5 (hippocampus) and 6 (striatum). Notably, basal levels of extracellular ACh in hippocampus were unchanged after icv-STZ (saline 8.71 ± 1.33 nM, low dose 7.29 ± 0.84 nM, high dose 7.48 ± 1.58 nM, $N = 6$; $p > .3$) (Table 1). Exploration in the open field approximately doubled ACh levels in the hippocampus, but increases were similar among the three experimental groups (Figure 5a). After 30 min in the open field, ACh levels were 16.82 ± 3.00 nM in controls, 16.78 ± 2.51 nM in the low-dose, and 21.57 ± 4.57 nM in the high-dose group ($N = 6$; $p > .3$) (Figure 5a). Two-way ANOVA of the time courses revealed no significant difference between groups.

On day 2, an infusion of scopolamine was used to increase ACh release. All groups responded to the treatment with a threefold increase in ACh levels (Figure 5b) and showed similar maximum increases at 75 min (saline 36.10 ± 5.94 nM, low-dose STZ 29.19 ± 8.17 nM, high-dose STZ 34.2 ± 6.31 nM; $N = 6$, $p > .3$). Again, two-way ANOVA revealed no significant difference between groups.

As the lack of cholinergic response seemed surprising, we repeated these experiments in the *Corpus striatum*, a brain area with rich cholinergic innervation that was exposed to STZ after i.c.v. administration. As shown in Figure 6, basal ACh levels in the striatum were higher than in the hippocampus but still similar between experimental groups ($p > .05$). Surprisingly, the highest ACh values were observed after high-dose STZ (Figure 6a). While the response to the open field was less prominent in the striatum than in the hippocampus, two-way ANOVA revealed a significant difference between high-dose STZ and saline which was strongest at time 90 min of the open field test ($p < .05$; Figure 6a). Similar to the hippocampal data, scopolamine caused a more than threefold increase in ACh release in the striatum, but STZ treatment did not modify the response of cholinergic neurons in this paradigm (Figure 6b).

To complement the results of the microdialysis study, we measured the cholinergic parameters ChAT and AChE in hippocampal and striatal homogenates and HACU (CHT-1) in the P2 fractions of hippocampus and striatum. After normalization to protein content, all cholinergic parameters were decreased in the hippocampus after high-dose STZ: HACU activity (−16%; $p = .3$), ChAT activity (−28%, $p < .01$), and AChE activity (−30%; $p < .01$) (Table 2). In contrast, in the striatum, ChAT activity was preserved while HACU (+31%, $p < .05$) and AChE activity (+7%; $p < .05$) were increased (Table 3).

3.4 | Single-cell sequencing analyses

The apparent lack of specific toxicity toward cholinergic neurons brought up questions about the mechanism of STZ toxicity in the

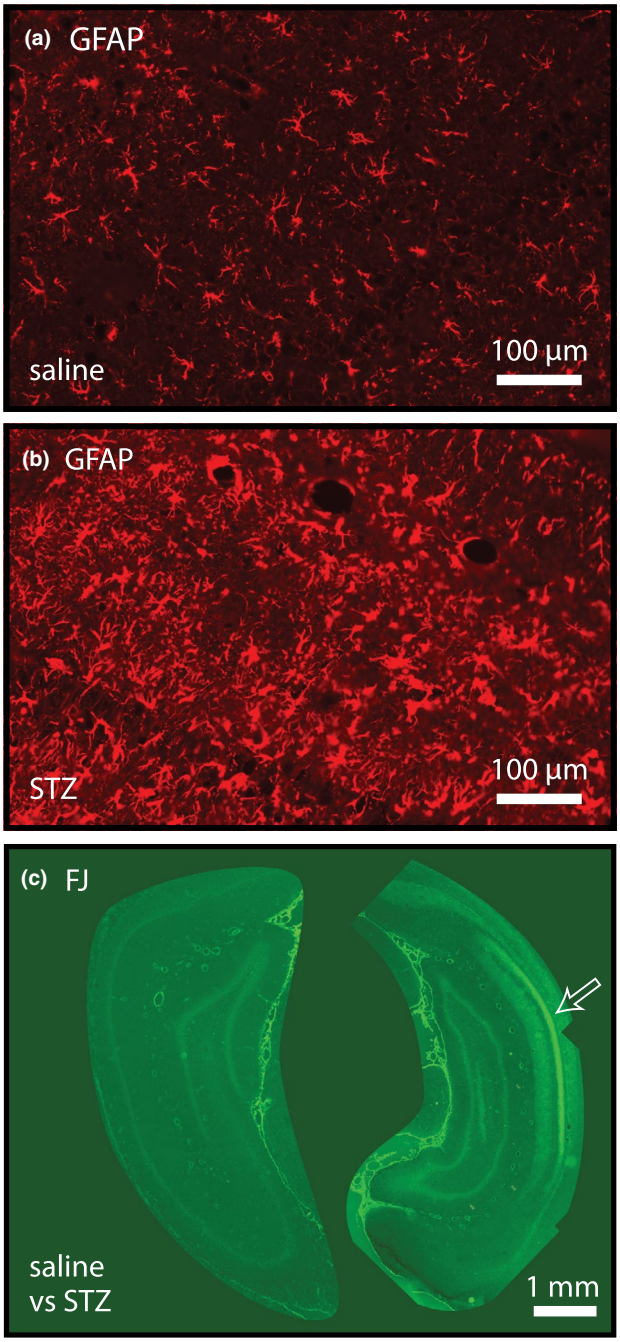

FIGURE 3 Coronal cryosections of the hippocampus (14 µm) at AP −5.6 mm from bregma. (a) Glial fibrillary acidic protein (GFAP) immunoreactivity in the rat hippocampus 21 days after i.c.v. injection of saline. (b) Strong GFAP immunoreactivity in rat hippocampus 21 days after i.c.v. injection of streptozotocin (STZ). (c) Lower magnification: Fluoro-Jade C staining illustrates extensive STZ-induced degeneration of the CA1 region (arrow). In the saline group, no signal was observed in the CA1 region

brain. Since, in the periphery, STZ-mediated toxicity depends on specific glucose transport (reportedly via GLUT2), we elected to analyze recent single-cell expression data with regard to cholinergic markers and the relevant glucose transport proteins. We used raw single-cell expression data of the adult mouse nervous system (Zeisel et al., 2018) to determine expression and correlation of cholinergic and glucose

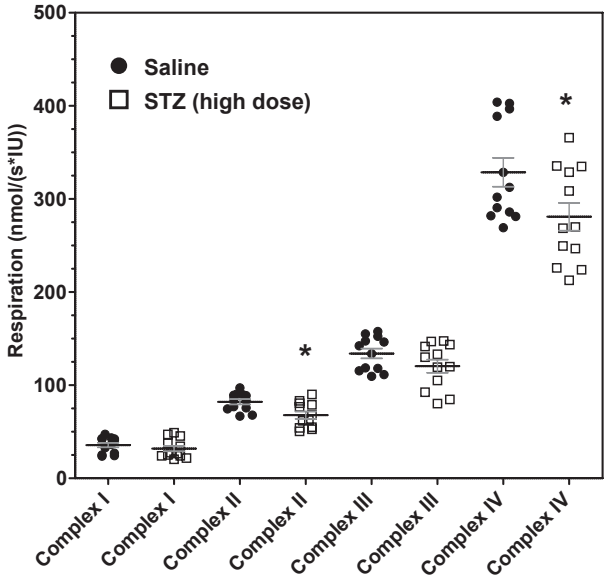

FIGURE 4 Mitochondrial respiration: Changes in oxygen flux in complexes I, II, III, and IV of the electron transport chain (ETC). Substrates, uncoupler and inhibitors were used to measure each complex as described in Methods. Raw data as obtained from respirometry were normalized to mitochondrial citrate synthase activity. Statistical analysis: Data are means ± *SEM* ($N = 12$ animals) and were analyzed by unpaired *t*-test. $^{*}p < .05$ compared to saline

transporter genes. Expression levels of cholinergic markers (AChE; ChAT; and SLC5A7, also known as CHT-1, the high-affinity choline transporter) and glucose transmembrane transporters (SLC2A1, SLC2A2, SLC2A3, and SLC2A4; also known as GLUT1, GLUT2, GLUT3, and GLUT4, respectively) in selected brain regions (hippocampus and striatum) were determined at single-cell level, and displayed via violin plot of $\log_2$(expression + 1) (Figure S3). The data show a widespread expression of AChE but a low expression of ChAT and CHT-1, as is consistent with the literature. Among the glucose transporters, GLUT 3 is widely expressed, GLUT1 and GLUT4 are found in hippocampus and striatum in small amounts, while GLUT2 mRNA is basically absent apart from the ventral striatum.

Correlation coefficients of expression of the selected genes were calculated for all 265 tissues of the cell-type-level data of the murine nervous system (Figure S4a), and at the single-cell-level for all neurons (Figure S4b) and for cholinergic neurons alone (Figure S4c; defined as expressing the vesicular ACh-transporter SLC18A3). We observed high correlations between ChAT and SLC5A7 (CHT-1) expression, indicating a joint expression predominantly in cholinergic neurons. Importantly, expression of AChE showed less correlation with either ChAT or CHT-1 expression, indicating AChE expression in many cell types of the murine nervous system. Non-neuronal cells seem to contribute significantly to AChE expression since AChE expression correlated poorly when all single neurons were compared (Figure S4b). Finally, SLC2A3 (GLUT3) showed the highest correlations with AChE, ChAT, and SLC5A7 (CHT-1), whereas SLC2A1 (GLUT1) showed a low correlation and SLC2A2 (GLUT2) and SLC2A4 (GLUT4) basically none.

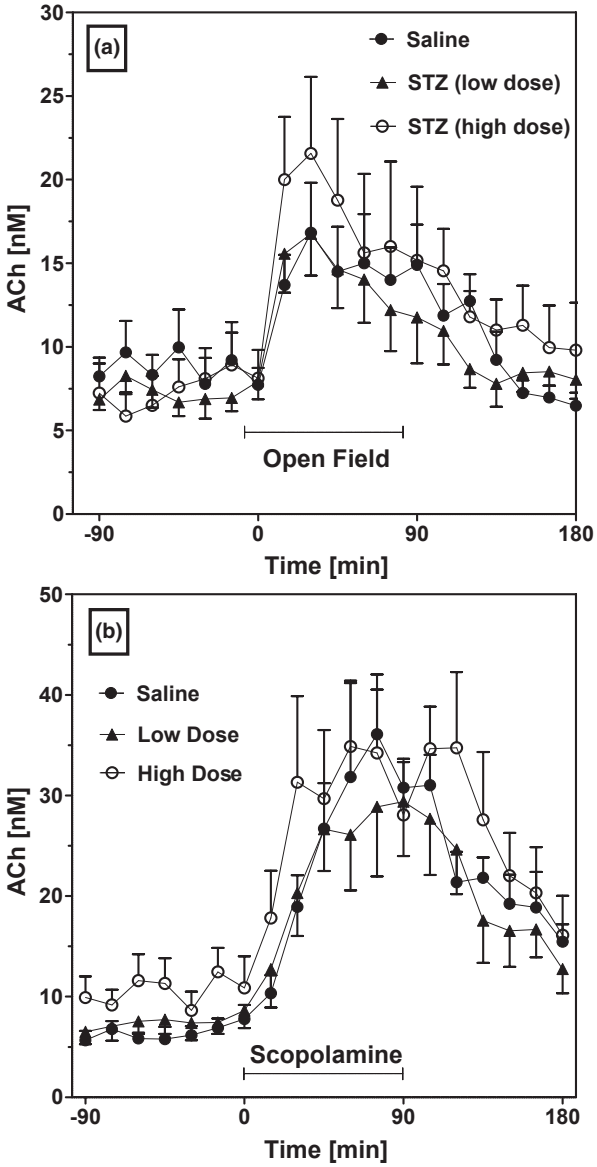

FIGURE 5 Acetylcholine (ACh) levels in rat hippocampal microdialysates during behavioral and cholinergic challenges. (a) Open field test (from time 0 until 90 min). (b) Infusion of scopolamine (1 μM) (from time 0 until 90 min). Data are means ± *SEM* (*N* = 6 animals) and were analyzed by two-way ANOVA with Bonferroni post-tests: (a) $F_{2,17} = 0.33$, $p = .72$; (b) $F_{2,17} = 1.09$, $p = .36$

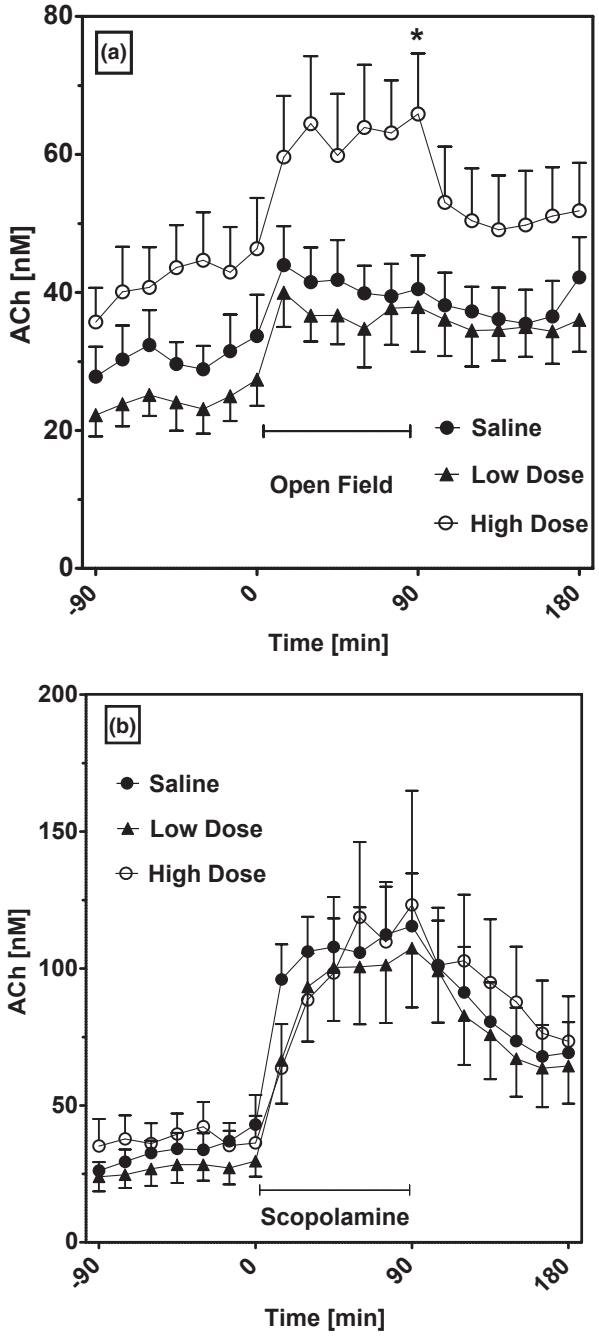

FIGURE 6 Acetylcholine (ACh) levels in rat striatal microdialysates during behavioral and cholinergic challenges. (a) Open field test (from time 0 until 90 min). (b) Infusion of scopolamine (1 μM) (from time 0 until 90 min). Data are means ± *SEM* (*N* = 8 animals) and were analyzed by two-way ANOVA with Bonferroni post-tests: (a), $F_{2,21} = 3.8$, $p = .04$; (b) $F_{2,23} = 0.16$, $p = .85$. *$p < .05$ compared to saline

4 | DISCUSSION

The present data can be interpreted in two ways, namely, (a.) referring to STZ´s mechanism of action in the brain and (b.) to STZ´s effects on the central cholinergic system.

4.1 | Mechanism of action of streptozotocin in the brain

Reduced glucose consumption is an early sign of Alzheimer´s disease (AD), preceding clinical symptoms of memory loss and dementia by several years. As diabetes is known to increase the risk for AD by 1.5- to 2-fold, AD has been hypothesized to be an insulin-resistant state of the brain and has even been termed "diabetes type 3" (de la Monte, 2014). However, the connection among diabetes, insulin, and AD is far from proven (Salas & de Strooper, 2019; Schilling, 2016). While animal studies suggest a role for insulin in cognition, the situation in the human is more complex (Arnold et al., 2018; Biessels &

Reagan, 2015). Streptozotocin (STZ) is a drug that, after systemic administration, induces experimental type 1 diabetes in rats and mice by preferential uptake via GLUT2 glucose transporters into pancreatic ß-cells and subsequent cellular toxicity (alkylation and DNA damage) (Grieb, 2016). The icv-STZ model was developed to imitate this mechanism in the brain, although there is little evidence that the brain contains insulin-producing cells (Blazquez, Velazquez, Hurtado-Carneiro, & Ruiz-Albusac, 2014). The mechanism of action of STZ in the brain, however, is far from clear (Grieb, 2016). According to present knowledge, the glucose transporters GLUT2 and the insulin-dependent GLUT4 are present in the brain in very low amounts, whereas the glial GLUT1 and the neuronal GLUT3 are highly expressed. Our analysis of murine single-cell expression data confirms that GLUT2 is basically absent from the brain. While GLUT4 was suggested to play a major role in insulin action in the brain (McNay and Pearson-Leary, 2020), our analysis shows low expression and no correlation of GLUT4 expression with cholinergic markers. More likely, then, STZ may enter brain cells through the ubiquitous GLUT1 and GLUT3 transporters. Hence, a specific effect of STZ on a subset of brain cells is unlikely; more likely, many neuronal cell types as well as glial cells will be exposed to STZ toxicity after i.c.v. injection. According to our analysis (Figure S4), GLUT3 expression has a significant correlation with cholinergic genes, hence, STZ may enter cholinergic cells via GLUT3 (SLC2A3).

Following icv-STZ, we found GFAP-positive staining in all treated rats which indicates astrogliosis. This finding corroborates previous reports of reactive gliosis in this model (Knezovic et al., 2017; Mishra, Singh, Shukla, & Shukla, 2018; Rai, Kamat, Nath, & Shukla, 2014; Santos, Mazucanti, Xavier, & Torrão, 2012). We also found cells that stained positive for Fluoro-Jade C (FJ) in some but not all of the animals. Fluoro-Jade C is an acidic dye postulated to label basic molecules of degenerating neurons. It is known that FJ staining is strongly time dependent and may disappear after several days (Santos et al., 2012); this may explain the lack of staining in several animals. Additional signs of neurodegeneration were observed in long-lasting studies (Knezovic et al., 2015; Salkovic-Petrisic et al., 2011). These signs of toxicity may not have shown up in our study because we used the most popular regimen, i.e., testing of the animals 3 weeks after STZ administration. Importantly, icv-STZ rats gained very little weight for 2 weeks after administration of STZ, a finding that clearly reflects the toxicity of the compound. It is remarkable that throughout our experiments, the low dose of 0.6 mg/kg (once) did not cause any significant changes in the parameters measured; the high dose (twice 1.5 mg/kg) was required to induce toxicity. We also found signs of toxicity in the microdialysis study: Increases in choline and glycerol are known to signify membrane damage because they are breakdown products of cellular membranes (Klein, 2000; de Lima Oliveira et al., 2014). Taken together, our findings demonstrate that the usual dose of icv-STZ induces severe toxicity for 10 days followed by a recovery period, but even after 3 weeks, signs of neurodegeneration and astrogliosis are clearly visible.

Although abnormalities in glucose metabolism are implicitly assumed to occur in the STZ model, we here show that extracellular glucose levels in the brain are not affected by icv-STZ. We found a decrease in lactate levels after icv-STZ, but the effect did not reach statistical significance. In the absence of ischemia, lactate in the brain is mainly formed by astrocytes to supply neurons with metabolic energy (Dienel, 2012), and a reduction in lactate may be caused by glial dysfunction induced by astrogliosis (see above). Similarly, decreased lactate levels were observed in other AD models (Lu et al., 2015; Zhang et al., 2018).

We also measured glucose and lactate levels in dialysates during behavioral and pharmacological stimulation. Similar to earlier findings (Hartmann, Kiewert, & Klein, 2010), glucose levels did not change significantly, whereas lactate levels were increased during the open field test. The latter finding is probably as a result of neuronal activation during exploration (Hartmann et al., 2010). Again, all treatment groups responded similarly during stimulation.

To further characterize metabolic dysfunction in the icv-STZ model, we isolated hippocampal mitochondria and determined the activities of the complexes of the electron transport chain. For this purpose, we used high-resolution respirometry combined with substrates-uncoupler-inhibitors titration (SUIT) protocol developed previously (Hagl et al., 2013). Similar to previous work (Correia et al., 2013; Paidi et al., 2015), we found reduced oxygen consumption in hippocampal mitochondria. In our hands, all complexes showed reduced activity with the most significant changes occurring in complexes II and IV. Reductions in complex I were not statistically significant, and in agreement with this finding, we did not observe a change in isoprostane levels in dialysate samples which means that oxidative stress was not visibly increased. Of note, a major reduction in mitochondrial activity would be expected to reduce pyruvate consumption in the TCA cycle and to increase the lactate/pyruvate ratio, a response that was not observed here.

4.2 | Effects of streptozotocin on central cholinergic transmission

Central cholinergic dysfunction is an important characteristic of AD because, first, it strongly correlates with clinical symptoms of dementia and, second, it is the target of the currently used drug treatment with AChE inhibitors (Ballinger et al., 2016; Mohr, Zimmermann, & Klein, 2013). Previous reports of reductions in ChAT activities or increases in AChE in the icv-STZ model seemed to point toward a cholinergic dysfunction. However, the observed changes were often small and inconsistent (see Introduction). Some studies reported a significant increase in AChE activity (e.g., Costa et al., 2016; Sorial & El-Sayed, 2017) while others found a decrease in hippocampal AChE gene expression (Chen et al., 2012). The factors influencing AChE expression are well known (Soreq & Seidman, 2001), however, our measurements in tissue homogenates do not allow a distinction between changes in expression in specific cell types.

In the present study, we used microdialysis to measure extracellular levels of ACh and its changes during behavioral or pharmacological stimulation. Surprisingly, basal levels of extracellular ACh

(approx. 7 nM) in the hippocampal microdialysates were unchanged 3 weeks after icv-STZ. Exploration of the open field caused an increase in ACh release that was more pronounced in hippocampus than in striatum. However, ACh release was not impaired after icv-STZ; in fact, there were slightly higher ACh levels in the striatal dialysates after icv-STZ. In both brain regions, the infusion of scopolamine caused a several-fold increase in ACh levels as a result of the blockade of negative feedback through M2/M4-type receptors (Mohr et al., 2013). Again, the response of the cholinergic pathways was identical in all groups. Evidently, icv-STZ did not cause a major dysfunction of central cholinergic pathways.

Our measurements of cholinergic parameters and the bioinformatic analyses of murine single-cell data allow us to draw a differential picture of the cholinergic response in two brain areas with prominent cholinergic innervation, namely, hippocampus and striatum. Two limitations must be noted for this analysis. First, as discussed by Grieb (2016), the pattern of damage is influenced by the limited diffusion of STZ from the ventricular space. In preliminary experiments (data not shown), we found that a dye-injected i.c.v. reached hippocampal and striatal tissue but not the basal forebrain (e.g., the septal area where hippocampal cholinergic fibers originate). This corroborates an earlier study that also failed to see cholinergic damage in the septal area (Terwel et al., 1995). Second, the analyzed single-cell data were of murine origin, and for the present purpose we have to hypothesize that the expression of cholinergic transcripts and glucose transporters is similar in rats and mice.

These limitations notwithstanding, we can conclude from our data that icv-STZ causes a mild reduction in cholinergic parameters in the hippocampus which is, however, not reflected in a change in extracellular ACh levels. It seems likely that the reduction in ChAT and HACU activities is caused by STZ entering cholinergic axons or nerve terminals in the hippocampus through GLUT3 transporters. Subsequent toxicity may damage some cholinergic neurons which may cause a reduction in ChAT activity which is, however, not rate limiting for ACh synthesis and release (Brandon et al., 2004; König, Berlin, et al., 2018). Concomitantly, STZ may also enter neighboring neurons or astrocytes through GLUT1 or GLUT3 and reduce the expression of AChE. AChE is more closely coupled to extracellular ACh levels (Erb et al., 2001), but a reduction in AChE would evidently increase extracellular ACh. We hypothesize that the small changes in ChAT and AChE activities do not influence ACh synthesis and degradation. Alternatively, the small reduction of ChAT activity may lower ACh release, but this effect may be balanced by the small reduction in AChE activity which would prolong its lifetime. Clearly, a cholinergic dysfunction does not result from these effects.

The cholinergic system of the striatum is quite different from that of the hippocampus. The striatum contains short projecting cholinergic interneurons that seem to be spared from STZ toxicity. ChAT activity is unchanged while HACU and AChE are slightly increased which may indicate a somewhat faster cholinergic firing rate, accompanied by a minor increase in ACh hydrolysis. Extracellular levels of ACh are unchanged or, in the open field, slightly increased after icv-STZ. The findings in the striatum clearly indicate that cholinergic neurons are not severely damaged by STZ. It seems possible that some other neurons in the vicinity of cholinergic synapses may be damaged and may influence the cholinergic firing rate; however, our preliminary attempts to demonstrate GABAergic toxicity were unsuccessful. Again, some damage to glial cells may also indirectly affect cholinergic striatal interneurons.

5 | CONCLUSION

Taken together, these data show preserved cholinergic function 3 weeks after icv-STZ administration. In the hippocampus, cholinergic nerve terminals may sustain some minor damage that does not, however, impair their ability to release ACh during behavioral or pharmacological stimulation. In the striatum, cholinergic interneurons seem to be protected from STZ toxicity. In contrast, we saw clear signs of astrogliosis, neurodegeneration, and some impairment of energy metabolism. Hence, the icv-STZ model lacks an important component of AD pathology, namely, cholinergic dysfunction, and, therefore, is a poor model of human AD. It may be more correctly qualified as an animal model of hippocampal gliosis and toxicity.

ACKNOWLEDGMENTS

The authors wish to thank Dr Magdalena König for assistance with microdialysis, Dr Anna Thinnes for assistance with the oxygraph, Dr Jonas Petersen for assistance with immunofluorescence, and Helene Lau for cholinergic marker measurements and excellent technical assistance. The study was supported by internal funds of Goethe University to Dr Klein and a stipend from LPDP (Indonesia Endowment Fund for Education, Ministry of Finance, Republic of Indonesia) to T. Yuliani. Open access funding enabled and organized by Projekt DEAL.

All experiments were conducted in compliance with the ARRIVE guidelines.

CONFLICT OF INTEREST

The authors have no conflicts of interests to declare.

ORCID

Tri Yuliani https://orcid.org/0000-0002-7271-6580
Sebastian Lobentanzer https://orcid.org/0000-0003-3399-6695
Jochen Klein https://orcid.org/0000-0001-6971-3381

REFERENCES

Arnold, S. E., Arvanitakis, Z., Macauley-Rambach, S. L., Koenig, A. M., Wang, H.-Y., Ahima, R. S., … Nathan, D. M. (2018). Brain insulin resistance in type 2 diabetes and Alzheimer disease: Concepts and conundrums. *Nature Reviews Neurology*, *14*, 168–181. https://doi.org/10.1038/nrneurol.2017.185

Ballinger, E. C., Ananth, M., Talmage, D. A., & Role, L. W. (2016). Basal forebrain cholinergic circuits and signaling in cognition and cognitive decline. *Neuron*, *91*, 1199–1218. https://doi.org/10.1016/j.neuron.2016.09.006

Banks, W. A., Owen, J. B., & Erickson, M. A. (2014). Insulin in the brain: There and back again. *Pharmacology & Therapeutics*, *136*, 82–93.

Biessels, G. J., & Reagan, L. P. (2015). Hippocampal insulin resistance and cognitive dysfunction. *Nature Reviews. Neurology*, *16*, 660–671.

Blazquez, E., Velazquez, E., Hurtado-Carneiro, V., & Ruiz-Albusac, J. M. (2014). Insulin in the brain: Its pathophysiological implication for states related with central insulin resistance, type 2 diabetes and alzheimer´s disease. *Frontiers in Endocrinology*, *5*, 161.

Bradford M. M. (1976) A rapid and sensitive method for the quantitation of microgram quantities of protein utilizing the principle of protein-dye binding. *Analytical Biochemistry 72*(1–2), 248–254. http://dx.doi.org/10.1016/0003-2697(76)90527-3

Brandon, E. P., Mellott, T., Pizzo, D. P., Coufal, N., D'Amour, K. A., Gobeske, K., … Blusztajn, J. K. (2004). Choline transporter 1 maintains cholinergic function in choline acetyltransferase haploinsufficiency. *Journal of Neuroscience*, *24*, 5459–5466. https://doi.org/10.1523/JNEUROSCI.1106-04.2004

Cavanaugh, S. E., Pippin, J. J., & Barnard, N. D. (2014). Animal models of alzheimer disease: Historical pitfalls and a path forward. *Altex*, *31*, 279–302. https://doi.org/10.14573/altex.1310071

Chen, Y., Tian, Z., Liang, Z., Sun, S., Dai, C. I., Lee, M. H., … Gong, C. X. (2012). Brain gene expression of a sporadic (icv-STZ mouse) and a familial mouse model (3xTg-AD mouse) of Alzheimer's disease. *PLoS One*, *7*, 12. https://doi.org/10.1371/journal.pone.0051432

Clarke, J. R., Ribeiro, F. C., Frozza, R. L., De Felice, F. G., & Lourenco, M. V. (2018). Metabolic dysfunction in Alzheimer´s disease: From basic neurobiology to clinical approaches. *Journal of Alzheimer's Disease*, *64*, S405–S426. https://doi.org/10.3233/JAD-179911

Correia, S. C., Santos, R. X., Santos, M. S., Casadesus, G., Lamanna, J. C., Perry, G., … Moreira, P. I. (2013). Mitochondrial abnormalities in a streptozotocin-induced rat model of sporadic alzheimer's disease. *Current Alzheimer Research*, *10*, 406–419.

Costa, M., Bernardi, J., Fiuza, T., Costa, L., Brand, R., & Pereira, M. E. (2016). N-acetylcysteine protects memory decline induced by streptozotocin in mice. *Chemico-Biological Interactions*, *253*, 10–17. https://doi.org/10.1016/j.cbi.2016.04.026

de la Monte, S. M., & Tong, M. (2014). Brain metabolic dysfunction at the core Alzheimer's disease. *Biochemical Pharmacology*, *88*, 548–559.

de Lima Oliveira, M., Kairalla, A. C., Fonoff, E. T., Martinez, R. C. R., Teixeira, M. J., & Bor-Seng-Shu, E. (2014). Cerebral microdialysis in traumatic brain injury and subarachnoid hemorrhage: State of the art. *Neurocritical Care*, *21*, 152–162.

Deeds, M. C., Anderson, J. M., Armstrong, A. S., Gastineau, D. A., Hiddinga, H. J., Jahangir, A., … Kudva, Y. C. (2011). Single dose streptozotocin induced diabetes: Considerations for study design in islet transplantation models. *Laboratory Animals*, *45*, 131–140. https://doi.org/10.1258/la.2010.010090

Dienel, G. A. (2012). Brain lactate metabolism: The discoveries and the controversies. *Journal of Cerebral Blood Flow and Metabolism*, *32*, 1107–1138.

Drummond, E., & Wisniewski, T. (2017). Alzheimer's disease: Experimental models and reality. *Acta Neuropathologica*, *133*, 155–175. https://doi.org/10.1007/s00401-016-1662-x

Ellman, G. L., Courtney, K. D., Andres, V., & Featherstone, R. M. (1961). A new and rapid colorimetric determination of acetylcholinesterase activity. *Biochemical Pharmacology*, *7*, 88–95.

Erb, C., Troost, J., Kopf, S., Schmitt, U., Löffelholz, K., Soreq, H., & Klein, J. (2001). Compensatory mechanisms enhance hippocampal acetylcholine release in transgenic mice expressing human acetylcholinesterase. *Journal of Neurochemistry*, *77*, 638–646. https://doi.org/10.1046/j.1471-4159.2001.00287.x

Fonnum, F. (1969). Radiochemical micro assays for the determination of choline acetyltransferase and acetylcholinesterase activities. *The Biochemical Journal*, *115*, 465–472. https://doi.org/10.1042/bj1150465

Gerfen, C. R. (2003). *Basic neuroanatomical methods, in Curr. Protoc. Neurosci., Chapter 1: Unit 1.1*. New York: John Wiley & Sons.

Gnaiger, E. (2014). *Mitochondrial Pathways and Respiratory Control: An Introduction to OXPHOS Analysis*. Innsbruck: Oroboros Instruments Corp.

Grieb, P. (2016). Intracerebroventricular streptozotocin injections as a model of Alzheimer's disease: In search of a relevant mechanism. *Molecular Neurobiology*, *53*, 1741–1752. https://doi.org/10.1007/s12035-015-9132-3

Grillo, C. A., Piroli, G. G., Lawrence, R. C., Wrighten, S. A., Green, A. J., Wilson, S. P., … Reagan, L. P. (2015). Hippocampal insulin resistance impairs spatial learning and synaptic plasticity. *Diabetes*, *64*, 3927–3936. https://doi.org/10.2337/db15-0596

Hagl, S., Kocher, A., Schiborr, C., Eckert, S. H., Ciobanu, I., Birringer, M., … Eckert, G. P. (2013). Rice bran extract protects from mitochondrial dysfunction in guinea pig brains. *Pharmacological Research*, *76*, 17–27.

Hartmann, J., Kiewert, C., & Klein, J. (2010). Neurotransmitters and energy metabolites in amyloid-bearing APP SWExPSEN1dE9 mouse brain. *Journal of Pharmacology and Experimental Therapeutics*, *332*, 364–370.

Hellweg, R., Nitsch, R., Hock, C., Jaksch, M., & Hoyer, S. (1992). Nerve growth factor and choline acetyltransferase activity levels in the rat brain following experimental impairment of cerebral glucose and energy metabolism. *Journal of Neuroscience Research*, *31*, 479–486. https://doi.org/10.1002/jnr.490310310

Hoyer, S. (1998). Is sporadic Alzheimer disease the brain type of non-insulin dependent diabetes mellitus? A Challenging Hypothesis. *Journal of Neural Transmission*, *105*, 415–422. https://doi.org/10.1007/s007020050067

Imran, I., Hillert, M. H., & Klein, J. (2015). Early metabolic responses to lithium/pilocarpine-induced status epilepticus in rat brain. *Journal of Neurochemistry*, *135*, 1007–1018. https://doi.org/10.1111/jnc.13360

Kallenborn-Gerhardt, W., Lu, R., Bothe, A., Thomas, D., Schlaudraff, J., Lorenz, J. E., … Schmidtko, A. (2014). Phosphodiesterase 2A localized in the spinal cord contributes to inflammatory pain processing. *Anesthesiology*, *21*, 372–382. https://doi.org/10.1097/ALN.0000000000000270

Klein, J. (2000). Membrane breakdown in acute and chronic neurodegeneration: Focus on choline-containing phospholipids. *Journal of Neural Transmission*, *107*, 1027–1063. https://doi.org/10.1007/s007020070051

Knezovic, A., Loncar, A., Homolak, J., Smailovic, U., Barilar, J. O., Ganoci, L., … Salkovic-Petrisic, M. (2017). Rat brain glucose transporter-2, insulin receptor and glial expression are acute targets of intracerebroventricular streptozotocin: Risk factors for sporadic Alzheimer's disease? *Journal of Neural Transmission*, *124*, 695–708. https://doi.org/10.1007/s00702-017-1727-6

Knezovic, A., Osmanovic-Barilar, J., Curlin, M., Hof, P. R., Simic, G., Riederer, P., & Salkovic-Petrisic, M. (2015). Staging of cognitive deficits and neuropathological and ultrastructural changes in streptozotocin-induced rat model of Alzheimer's disease. *Journal of Neural Transmission*, *122*, 577–592. https://doi.org/10.1007/s00702-015-1394-4

Koch, K., Berressem, D., Konietzka, J., Thinnes, A., Eckert, G., & Klein, J. (2017). Hepatic ketogenesis induced by middle cerebral artery occlusion in mice. *Journal of the American Heart Association*, *7*, 1–10.

König, M., Berlin, B., Schwab, K., Frahm, S., Theuring, F., Wischik, C. M., … Klein, J. (2018). Increased cholinergic response in α-synuclein transgenic mice (h-α-SynL62). *ACS Chemical Neuroscience*, *10*, 1915–1922.

Lietsche, J., Gorka, J., Hardt, S., Karas, M., & Klein, J. (2014). Self-built microdialysis probes with improved recoveries of ATP and neuropeptides. *Journal of Neuroscience Methods*, *237*, 1–8.

Lu, W., Huang, J., Sun, S., Huang, S., Gan, S., Xu, J., … Jiang, X. (2015). Changes in lactate content and monocarboxylate transporter 2 expression in Aβ25-35-treated rat model of Alzheimer's disease. *Neurological Sciences*, *36*, 871–876.

Majkutewicz I., Kurowska E., Podlacha M., Myślińska D., Grembecka B., Ruciński J., … Wrona D. (2016) Dimethyl fumarate attenuates intracerebroventricular streptozotocin-induced spatial memory impairment and hippocampal neurodegeneration in rats. *Behavioural Brain Research 308*, 24–37. https://doi.org/10.12688/wellcomeopenres.14439.2

McNay, E. C., & Pearso-Leary, J. (2020). GluT4: A central player in hippocampal memory and brain insulin resistance. *Experimental Neurology*, *323*, 113076. https://doi.org/10.1016/j.expneurol.2019.113076

Mishra, S. K., Singh, S., Shukla, S., & Shukla, R. (2018). Intracerebroventricular streptozotocin impairs adult neurogenesis and cognitive functions via regulating neuroinflammation and insulin signaling in adult rats. *Neurochemistry International*, *113*, 56–68.

Mohr, F., Zimmermann, M., & Klein, J. (2013). Mice heterozygous for AChE are more sensitive to AChE inhibitors but do not respond to BuChE Inhibition. *Neuropharmacology*, *67*, 37–45. https://doi.org/10.1016/j.neuropharm.2012.11.001

Morgan, M., & Van Twisk, D. (2019). LoomExperiment: LoomExperiment container. R Package Version, 1.4.1.

Paidi, R., Nthenge-Ngumbau, D., Singh, R., Kankanala, T., Mehta, H., & Mohanakumar, K. (2015). Mitochondrial deficits accompany cognitive decline following single bilateral intracerebroventricular streptozotocin. *Current Alzheimer Research*, *12*, 785–795.

Paxinos, G., & Watson, C. (1998). *The rat brain in stereotaxic coordinates*, 4th ed. San Diego: Academic Press.

Rai, S., Kamat, P. K., Nath, C., & Shukla, R. (2014). Glial activation and post-synaptic neurotoxicity: The key events in streptozotocin (ICV) induced memory impairment in rats. *Pharmacology, Biochemistry and Behavior*, *117*, 104–117. https://doi.org/10.1016/j.pbb.2013.11.035

Salas, I. H., & de Strooper, B. (2019). Diabetes and Alzheimer's disease: A link not as simple as it seems. *Neurochemical Research*, *44*, 1271–1278. https://doi.org/10.1007/s11064-018-2690-9

Salkovic-Petrisic, M., & Hoyer, S. (2007). Central insulin resistance as a trigger for sporadic Alzheimer-like pathology: An experimental approach. *Journal of Neural Transmission*, *72*, 217–233.

Salkovic-Petrisic, M., Knezovic, A., Hoyer, S., & Riederer, P. (2013). What have we learned from the streptozotocin-induced animal model of sporadic Alzheimer's disease, about the therapeutic strategies in Alzheimer's research. *Journal of Neural Transmission*, *120*, 233–252. https://doi.org/10.1007/s00702-012-0877-9

Salkovic-Petrisic, M., Osmanovic-Barilar, J., Brückner, M. K., Hoyer, S., Arendt, T., & Riederer, P. (2011). Cerebral amyloid angiopathy in streptozotocin rat model of sporadic Alzheimer's disease: A long-term follow up study. *Journal of Neural Transmission*, *118*, 765–772. https://doi.org/10.1007/s00702-011-0651-4

Santos, T. O., Mazucanti, C. H. Y., Xavier, G. F., & Torrão, A. S. (2012). Early and late neurodegeneration and memory disruption after intracerebroventricular streptozotocin. *Physiology & Behavior*, *107*, 401–413. https://doi.org/10.1016/j.physbeh.2012.06.019

Schilling, M. A. (2016). Unraveling Alzheimer's: Making sense of the relationship between diabetes and Alzheimer's disease. *Journal of Alzheimer's Disease*, *51*, 961–977.

Schmued, L. C., Stowers, C. C., Scallet, A. C., & Xu, L. (2005). Fluoro-jade C results in ultra high resolution and contrast labeling of degenerating neurons. *Brain Research*, *1035*, 24–31. https://doi.org/10.1016/j.brainres.2004.11.054

Shoham, S., Bejar, C., Kovalev, E., Schorer-Apelbaum, D., & Weinstock, M. (2007). Ladostigil prevents gliosis, oxidative-nitrative stress and memory deficits induced by intracerebroventricular injection of streptozotocin in rats. *Neuropharmacology*, *52*, 836–843. https://doi.org/10.1016/j.neuropharm.2006.10.005

Soreq, H., & Seidman, S. (2001). Acetylcholinesterase – new roles for an old actor. *Nature Reviews Neuroscience*, *2*, 294–302.

Sorial, M. E., & El Sayed, N. S. E. D. (2017). Protective effect of valproic acid in streptozotocin-induced sporadic Alzheimer's disease mouse model: Possible involvement of the cholinergic system. *Naunyn-Schmiedeberg's Arch. Pharmacol.*, *390*, 581–593. https://doi.org/10.1007/s00210-017-1357-4

Terwel, D., Prickaerts, J., Meng, F., & Jolles, J. (1995). Brain enzyme activities after intracerebroventricular injection of streptozotocin in rats receiving acetyl-L-carnitine. *European Journal of Pharmacology*, *287*, 65–71.

Wickham, H. (2016). *ggplot2: Elegant Graphics for Data Analysis*, 2nd ed. New York: Springer.

Zeisel, A., Hochgerner, H., Lönnerberg, P., Johnsson, A., Memic, F., van der Zwan, J., … Linnarsson, S. (2018). Molecular architecture of the mouse nervous system. *Cell*, *174*, 999–1014. https://doi.org/10.1016/j.cell.2018.06.021

Zhang, M., Cheng, X., Dang, R., Zhang, W., Zhang, J., & Yao, Z. (2018). Lactate deficit in an Alzheimer disease mouse model: The relationship with neuronal damage". *Journal of Neuropathology and Experimental Neurology*, *77*, 1163–1176.

SUPPORTING INFORMATION

Additional supporting information may be found online in the Supporting Information section.

How to cite this article: Yuliani T, Lobentanzer S, Klein J. Central cholinergic function and metabolic changes in streptozotocin-induced rat brain injury. *J. Neurochem.* 2020;00:1–13. https://doi.org/10.1111/jnc.15155